Available online at www.sciencedirect.com
SCIENCE DIRECT®
International Journal of Heat and Fluid Flow 26 (2005) 264–275
International Journal of HEAT AND FLUID FLOW
www.elsevier.com/locate/ijhff

A new technique for dynamic heat transfer measurements and flow visualization using liquid crystal thermography

A. David Ochoa [a], James W. Baughn [a,*], Aaron R. Byerley [b]

[a] Department of Mechanical and Aeronautical Engineering, One Shields Avenue, University of California, Davis, CA 95616-5294, USA
[b] Department of Aeronautics, United States Air Force Academy, CO 80840-6222, USA

Received 8 January 2004; accepted 3 August 2004
Available online 7 October 2004

Abstract

A new technique for dynamic heat transfer coefficient measurements and flow visualization is described. This technique uses a surface with a low thermal mass (a thin tissue) embedded with thermochromic liquid crystals (TLCs) and heated uniformly with infrared radiation. For air heat transfer coefficient measurements, the frequency response is estimated at 0.3–0.5 Hz. Depending on the local heat transfer coefficient and the magnitude of its fluctuations, it is estimated that surface temperature fluctuations can be detected to 100 Hz. These surface temperature fluctuations are driven by changes in local heat transfer coefficients, caused by dynamic flow behavior such as vortex shedding, and are captured by video recordings of the hue of the liquid crystals. The video images provide time-dependent heat transfer coefficient distribution and time-dependent surface flow visualization. Two applications are used to illustrate this technique: flow on a surface downstream of a protruding cylinder in cross-flow with vortex shedding, and flow downstream of a shallow cylindrical surface dimple. Images of the time-dependent surface temperature distribution downstream of the protruding cylinder are presented. They show the fluctuations in the surface heat transfer coefficient due to vortex shedding. The temperature distributions downstream of the cylindrical dimple were found to be relatively steady within the frequency limits of this technique. Heat transfer coefficient contours are presented for this case.

1. Introduction and background

The objective of this research was to establish a new dynamic heat transfer coefficient measurement and surface flow visualization technique capable of measuring time-dependent fluctuations in heat transfer coefficients using liquid crystal (TLC) thermography. Two applications of this technique are presented: the flow behavior on a surface downstream of a protruding cylinder in cross-flow and that downstream of a shallow cylindrical dimple.

1.1. Heat transfer measurement techniques

Thermochromic liquid crystals (TLC's) change color with temperature due to a change in their molecular structure. The liquid crystals change from transparent at low temperatures, to red, yellow, green, blue and violet as the temperature is increased. At higher temperatures the liquid crystals return to the transparent state. Microencapsulation of the crystals by polymer spheres is used to make them more robust. By capturing RGB images of a surface coated with TLC's, it is possible to determine the surface temperature distribution from the hue distribution where the hue for each pixel is defined by

$$\mathrm{Hue} = \frac{1}{2\pi}\arctan\left[\frac{\sqrt{3}(\mathrm{G}-\mathrm{B})}{2\mathrm{R}-\mathrm{G}-\mathrm{B}}\right] \quad (1)$$

* Corresponding author. Tel.: +1 530 752 0580; fax: +1 530 752 4158.
E-mail address: jwbaughn@ucdavis.edu (J.W. Baughn).

0142-727X/$ - see front matter © 2004 Elsevier Inc. All rights reserved.
doi:10.1016/j.ijheatfluidflow.2004.08.002

Nomenclature

A	area of surface (m^2)
C_p	specific heat (J/kg K)
d	cylinder diameter (m)
D	dimple diameter (m)
f	shedding frequency (Hz)
h	convective heat transfer coefficient ($W/m^2 K$)
HSV	Hue, Saturation, Value color space
k	thermal conductivity (W/m K)
L	length of aluminum slug calorimeter (m)
Pr	Prandtl number
q''	heat flux (W/m^2)
Re	Reynolds number
RGB	Red, Green, Blue color space
RxCyW	liquid crystals having a red start temperature of x °C, with a bandwidth of y °C
x	characteristic length used for Nu, Re calculations (m)
St	Strouhal number for a cylinder (fd/V)
t	time (s)
T	temperature (°C)
ΔT	minimum discernable temperature change (°C)
V	freestream velocity (m/s)

Greeks

δ	film, paint and liquid crystal thickness (m)
ε	emissivity of surface
σ	Stefan–Boltzmann constant (5.67×10^{-8} $W/m^2 K^4$)
ξ	ratio defined by Eq. (10)
ρ	density (kg/m^3)
ω	frequency (rad/s)
τ	time constant (s)

Subscripts

∞	free stream air property
cond	conduction
conv	convection
cyl	cylinder
d	cylinder diameter
D	dimple diameter
f	final value
i	initial value
LC	liquid crystal
0	reference or average value
rad	radiation
s	surface
x	distance from leading edge

By their nature, TLC's reflect at wavelengths that are related to their temperature, and a temperature versus hue calibration may be done. Baughn (1995a) reviews heat transfer coefficient measurement methods using TLC's including the heated-coating method, variations of the transient method, and a uniform coating method.

The heated coating method can be used to measure heat transfer coefficients under steady state conditions. A nearly uniform heat flux is provided by covering an insulated surface with a thin conductive film which is electrically heated. When this film is coated with liquid crystals, lines of constant color indicate isotherms and the corresponding heat transfer coefficients. Heat flux is determined by electrical power measurement, with minor corrections for conduction and radiation losses. This technique was used by Mayhew et al. (2003) to establish the effect of freestream turbulence and blowing ratio on film cooling. The thermal mass of the substrate limited the rate at which a changing heat transfer coefficient can be measured with this technique.

The transient method, pioneered by Jones (1977), and also described by Baughn (1995a), is another method used to measure local heat transfer coefficients. This process uses a video recording to provide both time and location of the color play on a surface when it is exposed to a step change in the fluid temperature. The time that a surface takes to reach the temperature of the selected liquid crystal color play is used to calculate the local heat transfer coefficient. This method generally assumes that the local heat transfer coefficients are constant with time.

1.2. Flow visualization techniques

Flow visualization is useful for understanding flow nature and may provide both qualitative and quantitative information about 2D or 3D flow fields. Visualization techniques are especially important for validation and comparison to computational fluid dynamic (CFD) calculations. Van Dyke (1982) provides a collection of different types of flow visualization examples for many interesting applications. Three-dimensional flow visualization includes a variety of techniques including smoke methods (for air), dye methods (for water) and PIV and LDV methods. Surface flow visualization has most commonly been done with various types of tufts or chemical coatings. Tufts have a long history in flow studies, and can be as simple as attaching a piece of string to an aerodynamic surface. More recently, the development of thermal tufts has been used as a non-intrusive means of determining flow direction and separation as described by Baughn et al. (1995b). The method of thermal tufts involves producing a hot or cold (i.e., Byerley et al., 2002) spot on a surface that

has been coated with liquid crystal microcapsules. When exposed to a flow, the temperature distribution, displayed by the liquid crystals, appears as a tear drop shape pointing in the direction of the flow. Baughn et al. (1995b) used a laser thermal tuft, which was patented by the USAF (Rivir et al., 1999), to study flow separation on the suction side of a turbine blade. In the present research, the steady and the fluctuating surface heat coefficients provide a form of surface flow visualization.

2. New dynamic method for measuring heat transfer

A new technique for dynamic surface flow visualization and heat transfer coefficient (h) measurement is developed and described in this paper. This technique uses a surface with a low thermal mass substrate (a thin tissue stretched on a flat plate) which is embedded with thermochromic liquid crystals (TLCs) and is uniformly heated with incident infrared radiation. The surface temperature response, measured by the liquid crystals, is dependent on the thermal mass of the surface, h, and the percentage change in h. Surface temperature fluctuations are driven by changes in heat transfer coefficients, caused by dynamic flow behavior such as vortex shedding. Video recordings capture these fluctuations providing time-dependent surface flow visualization and the heat transfer coefficient distribution.

2.1. Model design and fabrication

The model base is machined from Plexiglas acrylic with a leading edge sanded to an elliptical nose. A 1 cm deep rectangular cavity with dimensions 12.7 cm × 15.24 cm is removed from the Plexiglas 10 cm from the elliptical leading edge. "Japanese tissue paper" (weight = 11.6 g/m^2) covers the model surface; it is folded over the edges of the model and secured with tape and glue. The model surface is then lightly sprayed with black paint (Hallcrest BB-G1, diluted 2:1 with water, added weight = 2.3 g per unit area). The black paint provides a high absorptivity (greater than 0.95) on the diffuse surface so that it will absorb most of the incident radiation. Spraying is done with multiple passes of the airbrush to ensure an even coating. When dry, microencapsulated thermochromic liquid crystals (added weight = 7.2 g per unit area) are airbrushed onto the surface using the same dilution ratio. As the model surface dries, the tissue shrinks leaving a taut, flat surface. Although no roughness measurements were made, the surface appears and feels smooth. High humidity causes the tissue to loosen and become wrinkled, however when heated it shrinks back to a taut surface.

The thin tissue provides a low mass per unit area and corresponding high response when insulated on the back. Air has a low thermal conductivity of 0.0263 W/mK and with a 1 cm deep cavity can be considered to have negligible free convection (Fig. 1).

For these measurements, a wind tunnel was used with a test section of 30 cm by 30 cm with a contraction ratio of 9.5:1. Tests were conducted at speeds of 3, 5, and 10 m/s.

Lighting and camera angle are important with liquid crystal measurements for repeatability in the temperature hue calibration. Fluorescent (cool white) lamps with ultraviolet filters were used in order to reduce UV damage to the liquid crystals.

2.2. Surface heating with infrared lamps

Heating is done with two infrared quartz lamps (38 cm long, 1.3 cm diameter) placed 10 cm from the model surface with 10 cm spacing from each other. They are located inside the test section of the wind tunnel. The

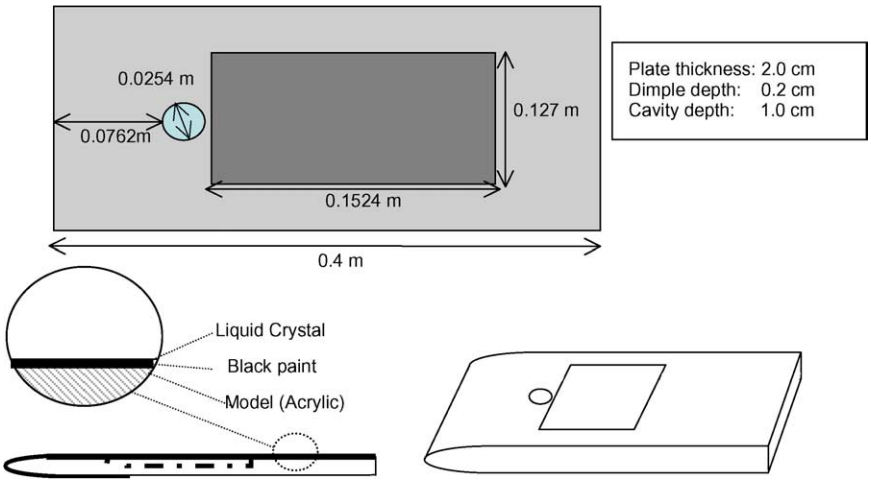

Fig. 1. Diagram of acrylic model.

lamps and holders produce approximately 3% blockage. Velocity measurements are made near the surface with the heaters in place. The 10 cm distance from the surface is far enough from the model to prevent flow interference over the length of the models. Infrared heating has been shown by Critoph et al. (1999) to be an effective way of providing a uniform heat flux without disturbing the flow field. They describe the technique of using radiative heat flux and liquid crystal thermography to measure local heat transfer coefficients using both steady state, and transient methods. Conclusions from their study were that using infrared heating gave heat transfer coefficient uncertainties within 10%, and that the steady state technique was preferred since it provided more accurate data.

Before heat transfer coefficients can be calculated the heat flux incident on the surface must be known. In the present study, a radiant lamp voltage squared (proportional to lamp power) versus incident heat flux calibration was performed using slug calorimetry. This was compared with predictions using laminar flow theory (in a test described later) and compares well as seen in Fig. 2. For the slug calorimetry, a piece of metal was inserted into the model with known dimensions and weight and a thermocouple attached. An aluminum shield was used to protect the slug from the radiant heating until quickly removed providing a step change in incident radiant heat flux. The absorbed heat flux is given by Eq. (2)

$$q''_{\text{absorbed}} = q''_{\text{incident}} - q''_{\text{transmitted}} - q''_{\text{reflected}} \tag{2}$$

Since the surface of the aluminum slug was covered with a flat black coating (graphite powder) with an absorptivity estimated at >0.95, the reflected radiant heat flux is neglected. However because the tissue paper is slightly transparent, we must account for the transmitted radiation. This is done by measuring the heat flux directly incident on the blackened slug, followed by a measurement in which the slug is placed behind a layer of tissue paper thereby measuring the transmitted radiant energy. The heat flux for both cases is found by conservation of energy at the surface:

$$q'' = \rho \cdot L \cdot C_p \frac{\mathrm{d}T}{\mathrm{d}t} \tag{3}$$

aluminum was chosen as the material for the slug.

With the heat flux known, the heat transfer coefficient, h, can be determined using the surface temperature given by the liquid crystals. The local heat transfer coefficient is given at a particular time for each location by

$$h = \frac{q''_{\text{conv}}}{T_s - T_\infty} \tag{4}$$

where q''_{conv} is the absorbed incident radiation by two quartz heat lamps with corrections for radiation emission from the surface.

Infrared heating is uniquely suited to this application since no additional heating material is added to the thermal mass of the surface for electrically heating. The heat flux is regulated by controlling the voltage on the radiant lamps with a variant power supply. Because the infrared lamps were located inside the wind tunnel test section for these experiments, care was taken to ensure that the lamps themselves did not disturb the flow near the test surface. Also, because the output of the lamps could be affected by the convective cooling of the flow, both lamps were encased inside Pyrex tubes. With strong lighting conditions the infrared lamps do not significantly affect the reflected Red component of the TLC's.

2.3. Calculated frequency response

This new method provides both transient heat transfer data and flow visualization. For the heat transfer data the method can best be characterized by a

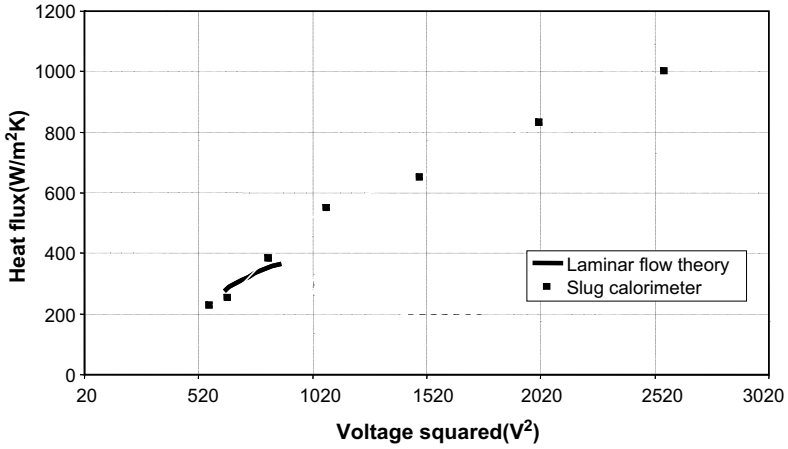

Fig. 2. Calibration of the slug calorimeter radiant heat flux against lamp voltage squared.

frequency response. For flow visualization there is a maximum observable frequency for flow fluctuations. Estimates of these frequencies are made below.

For heat transfer measurements, frequency response is dependent on the value of h and its percentage fluctuation, the range of the TLC selected, and the thermal mass of the substrate. The TLC's themselves have an estimated time constant of approximately 2 ms (see Ireland and Jones, 1986) which is not a factor here. For air, the maximum observable frequency due to flow fluctuations is estimated in the following analysis to be up to 100 Hz. The Nyquist sampling criteria, however, dictates the frequency response to be no more than half of the sampling rate. In this case a sampling rate of 30 frames per second limits the maximum frequency response to below 15 Hz. Though 15 Hz is the maximum, a more reasonable limit for the frequency response would 5 Hz (six frames per cycle).

To evaluate the dynamic response we start with an energy balance for an elemental tissue volume:

$$q''_{\text{net}} = \rho\delta C_p \frac{\mathrm{d}T}{\mathrm{d}t} = q''_{\text{r}} - h(T - T_\infty) \tag{5}$$

This assumes a lumped capacitance. Using $h = 150\,\text{W/m}^2\text{K}$, with an estimate of $\delta = 0.05$ mm and $k = 0.18\,\text{W/mK}$, the Biot number is approximately 0.04, thus this is a good assumption.

Eq. (5) has the general form of a first order instrument with a time constant τ given by

$$\tau = \frac{\rho\delta C_p}{h} \tag{6}$$

Analytically, the time constant and frequency response ($\omega = \frac{1}{2\cdot\pi\cdot\tau}$) are a function of only the substrate density, properties, and h. If h is constant, Eq. (5) can be easily solved giving:

$$T_{\text{f}} = \frac{q}{h} + T_\infty \tag{7}$$

which leads to:

$$T = \mathrm{e}^{-t/\tau}(T_{\text{i}} - T_{\text{f}}) + T_{\text{f}} \tag{8}$$

The tissue surface weighs 21.1 g/m^2 after both paint and liquid crystal have been applied. The specific heat C_p is estimated as 1.3 J/gK. The time constant can then be calculated using Eq. (6) for various h values as shown in Table 1.

In dynamic flow, h is not constant and may fluctuate cyclically due to vortex shedding as in the case of a cylinder in cross-flow. In this case we can assign h an oscillating nature:

$$h = h_0 + \Delta_h \cos(\omega t) \tag{9}$$

Solving Eq. (5) becomes more difficult now since h cannot be factored out of the integral so we used MatLab's ordinary differential equation solver. Using values corresponding to our tissue weight, estimated specific heat, and a free stream temperature of 20 °C, the temperature versus time solution is shown in Fig. 3.

Table 1
Time constant and frequency response for various values of h

h	τ (s)	ω (rad/s)
5	5.32	0.19
10	2.66	0.38
20	1.33	0.75
50	0.53	1.88
100	0.27	3.76
150	0.18	5.64

From this analysis, we may approximate the maximum observable frequency that the method can detect. To do this, the percent fluctuation of h is iteratively changed along with the minimum required temperature difference, ΔT, that will provide visualization. This may be determined by the color play range of the liquid crystal (1 °C is chosen for the present model). Thus, if the flow causes a 1 °C fluctuation of surface temperature, the liquid crystal will have gone through its entire color play. TLC's however, may resolve temperature differences much smaller, than its full color range when captured frames are converted into hue (i.e., as small as 0.1 °C for a 1 °C color play).

The parameter ξ is defined by Eq. (10).

$$\xi = \frac{\Delta T}{T_{\text{LC}} - T_\infty} \tag{10}$$

where ΔT is the minimum discernable temperature change for the liquid crystal. By accepting a smaller surface temperature change, we can detect higher frequencies. For the minimum detectable temperature difference of 0.1 °C, a liquid crystal activation temperature of 35 °C and a freestream temperature of 20 °C, ξ is equal to 0.0067. Fig. 4 shows that for an 80% fluctu-

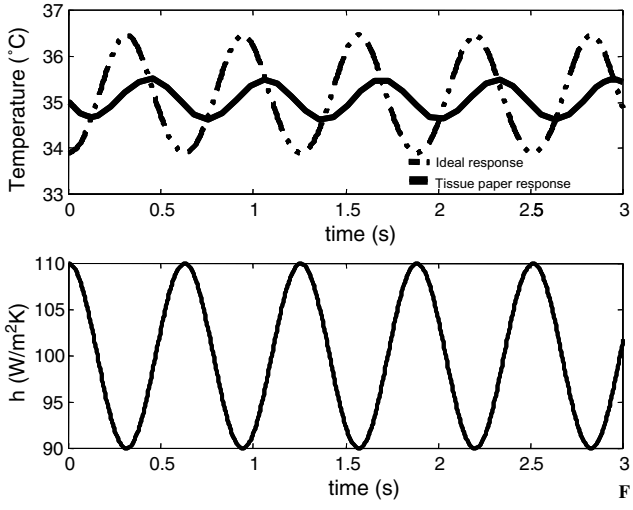

Fig. 3. Tissue paper temperature versus time for fluctuating h coefficient.

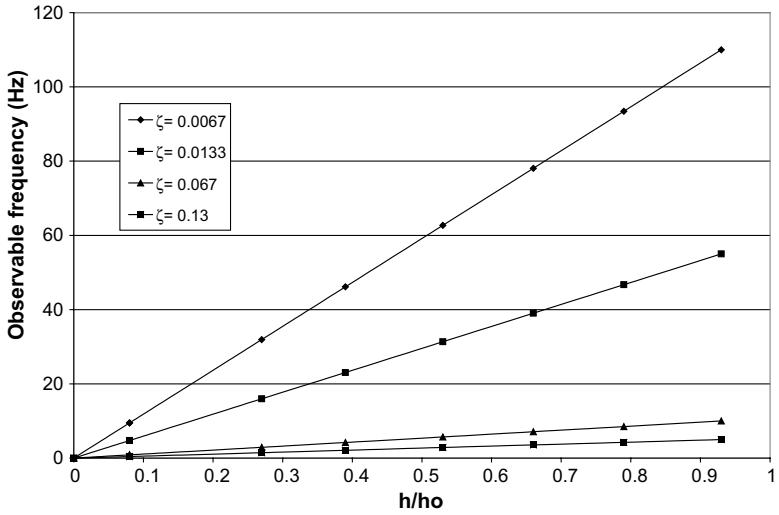

Fig. 4. The effect of heat transfer coefficient fluctuation and liquid crystal sensitivity on maximum observable frequency.

ation in h, the maximum observable frequency is approximately 100 Hz. Note that this is not affected by the actual value of h_0.

By the same iterative process, the frequency response for heat transfer coefficient measurements can also be determined. The attenuation of a first order system is given by Eq. (11).

$$\text{Attenuation} = \frac{\Delta T_{\text{measured}}}{\Delta T_{\text{input}}} = \frac{1}{\sqrt{1+\omega^2\tau^2}} \tag{11}$$

The frequency response ω (rad/sec), is usually defined as the value that makes Eq. (11) equal to $\frac{1}{\sqrt{2}}$, which occurs when $\omega = \frac{1}{\tau}$. This gives the system a standard 3 dB of attenuation (*Note*: in Fig. 3 the attenuation is approximately 50% or 6 dB). Using Matlab once again to determine the frequency response for a cyclical h, the maximum frequency response for 3 dB of attenuation can be found.

Fig. 5 depicts the frequency response where the temperature fluctuation attenuation is equal to $\frac{1}{\sqrt{2}}$ (3 dB) as a function of percent change in h. Measurements at higher frequencies may still be made with this technique, however the attenuation must be known for corrections to the data.

2.4. Demonstration of observable frequencies

To test the observable frequency of the method, a disturbance to the flow at a known rate is applied. A paddle wheel was inserted just upstream of the cavity (it was rotated with a shaft through the center of the dimple) and rotated at a speed to produce fluctuations

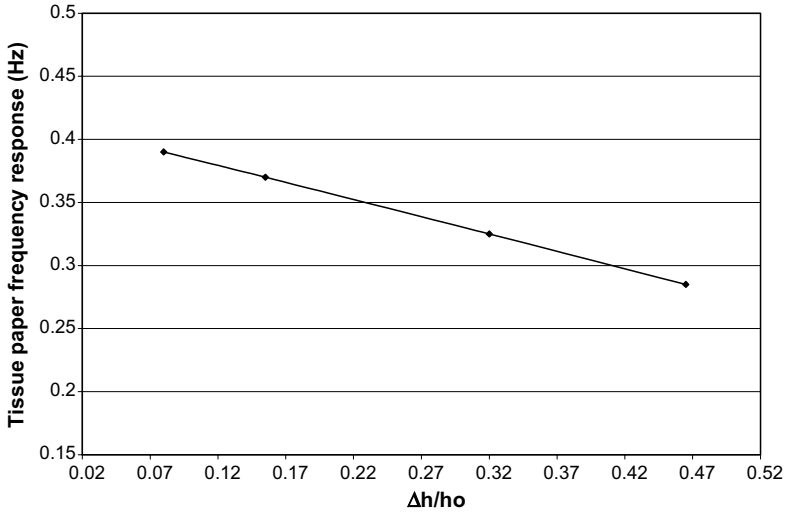

Fig. 5. The effect of heat transfer coefficient fluctuation on tissue paper frequency response (3 dB).

at the desired frequency. Rotating the paddle to produce surface fluctuations of 3.3 Hz, well within the sampling limits set by Nyquist, surface fluctuations were observed. Due to symmetry, two cycles are provided for every rotation, where a cycle is the paddle moving from its maximum blocking position to its minimum. The results of one cycle, equivalent to approximately 9 frames, are shown in Fig. 6. The circle in the images indicates one end of the paddle. The images were repeatable when the paddle returned to the same position in each cycle.

By inspection of Fig. 6 the individual paddle rotation frames do not show variation apparent to the human eye (though it is apparent in video). However by examining the hue of a single pixel or line of pixels, motion is evident between successive frames.

The fluctuation in the hue value for a single pixel (taken frame by frame) is shown in Fig. 7. These values are taken from above set of nine frames, and nine subsequent frames for a full rotation of the paddle (two complete cycles). The pixel observed was chosen at a location 0.57 m downstream from the center of the paddle, and is in the approximate location where the liquid crystals are yellow in color.

The magnitude of the hue change in Fig. 7 corresponds to an estimated 0.1° change in the surface temperature. Referring to Fig. 4, at a frequency of 3.3 Hz a 0.1° change in surface temperature, corresponds to a 5% variation in the heat transfer coefficient at this location.

2.5. Laminar boundary layer theory

In heat transfer measurements such as these, both hydrodynamic and thermal boundary layers are important factors. With infrared heating over the entire surface of the model, both the hydrodynamic and thermal boundary layers begin at the leading edge. The Nusselt number for a uniform heat flux boundary condition is given by (Incropera and DeWitt, 2002):

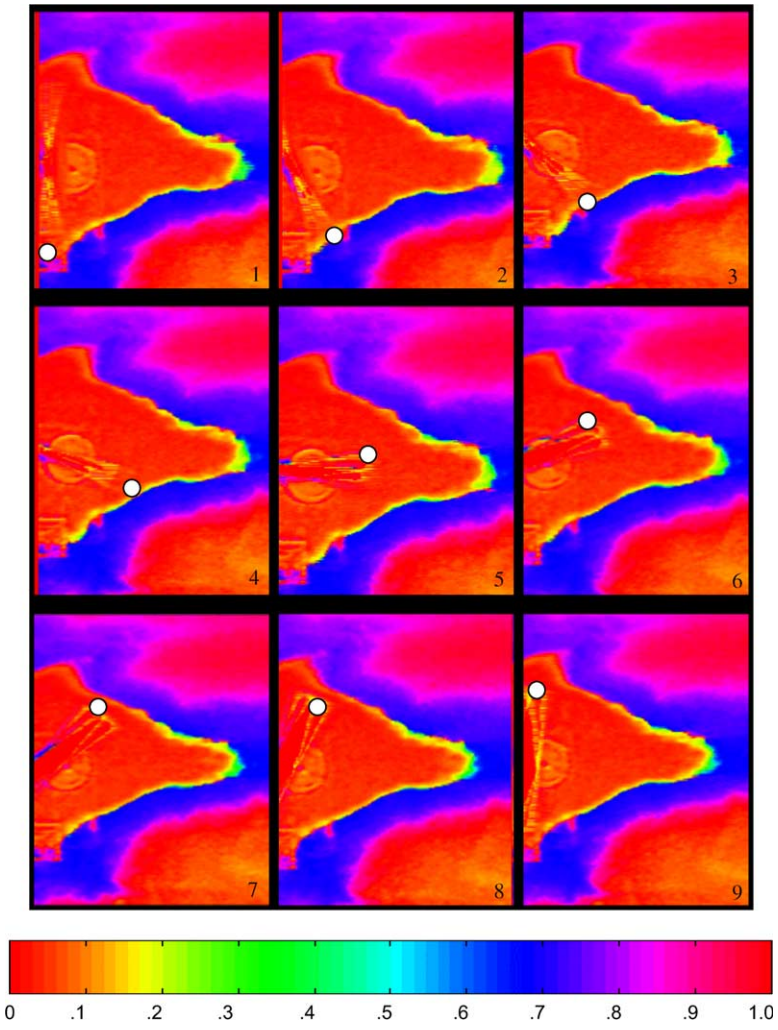

Fig. 6. Paddle wheel successive frames represented in Hue.

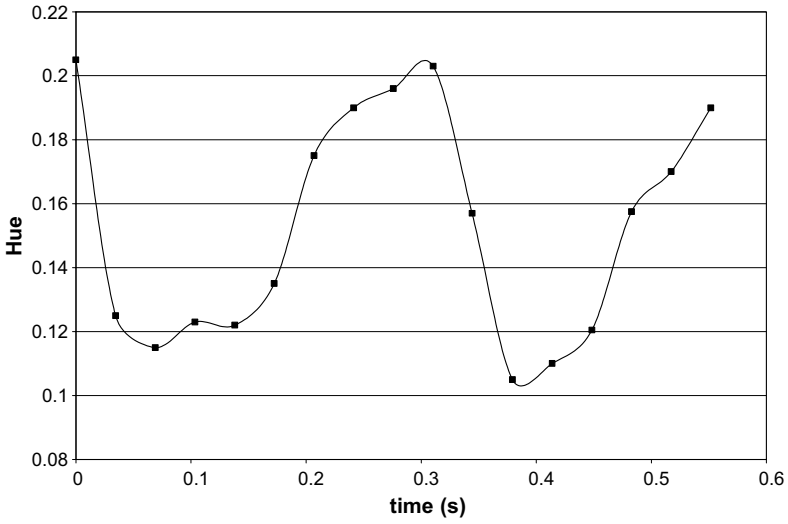

Fig. 7. The hue response of a single pixel to an oscillating heat transfer coefficient.

$$Nu = 0.453 * Re^{0.5} * Pr^{1/3} \tag{12}$$

with h coefficients based on laminar flow theory (Eq. (12), Fig. 8), it is possible to obtain heat flux values by rearranging Eq. (4) and solving for q''. Using the same flat plate with a dimple, data can be collected far enough away that the dimple should have no effect. The surface temperature, T_s, is found by noting the x location (and corresponding voltage applied to the heat lamps) where a line of constant yellow color is present spanwise along the model. This color represents the reported activation temperature of the liquid crystals (35 °C).

Because a surface also radiates energy (conductive losses are neglected due to insulation provided by the air filled cavity), a radiation heat transfer coefficient, h_r, is needed. The energy balance on the surface becomes:

$$q'' = q_{conv} + q_{rad} = (h + h_r) * (T_{LC} - T_\infty) \tag{13}$$

where radiation heat transfer coefficient is:

$$h_r = \varepsilon\sigma(T_{LC} + T_\infty) * (T_{LC}^2 + T_\infty^2) \tag{14}$$

The results showed a linear heat flux versus voltage squared correlation as shown in Fig. 9.

Though this correlation is based on laminar flow theory, heat flux results from the slug calorimetry described above agree well with this assumption (as shown in Fig. 2).

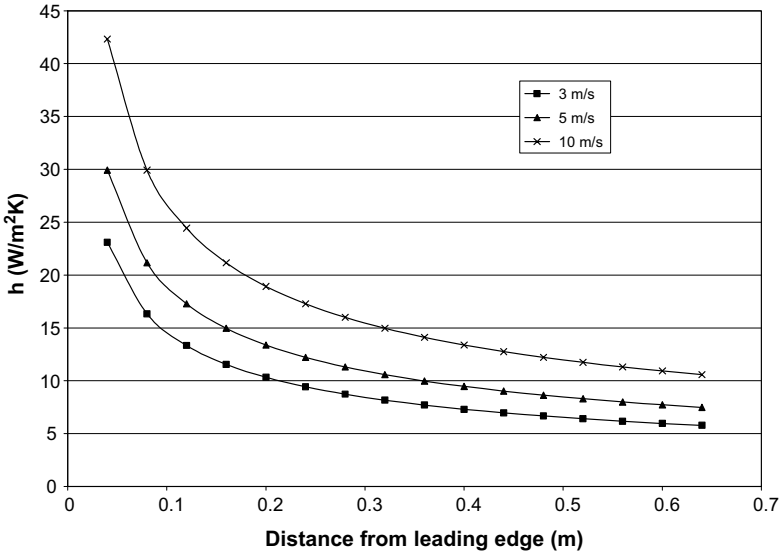

Fig. 8. Laminar flow heat transfer coefficients on a flat plate.

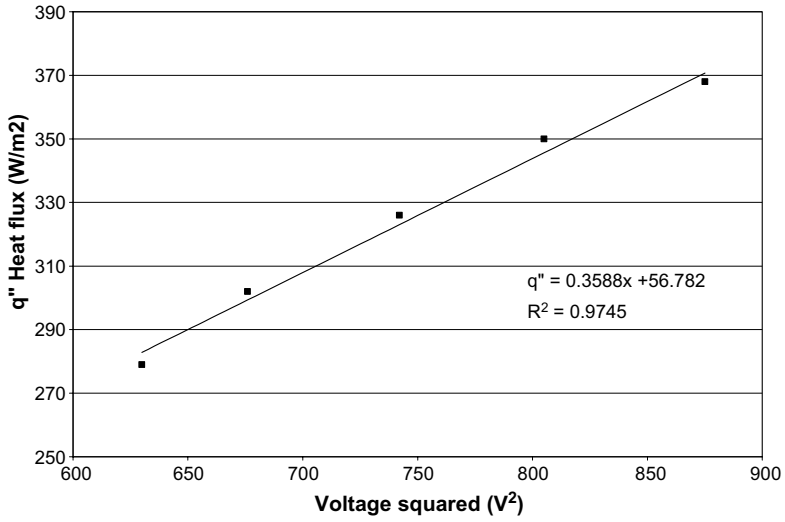

Fig. 9. Correlation of laminar theory heat flux with voltage squared.

2.6. Data acquisition

Video is taken at 30 frames per second using a Sony model XC-003 3-Chip RGB video camera. Images are captured through Red, Blue, and Green filters at 480×640 resolution. The camera signal is fed into a video capture card and converted into digital format. Once in digital format, the video may have individual frames extracted to a variety of file types. To capture the dynamic heat transfer into digital video (DV) for frame extraction, efficient and convenient storage on compact disc, and for frame by frame or slow motion playback, we used the uncompressed AVI format. For viewing dynamic fluctuations of the flow MPEG2 was used because of its smaller file sizes.

2.7. Data reduction—image processing

Once frame sequences were successfully extracted (into TIFF or PNG format), Matlab was used for image processing using a liquid Crystal Image Processing Toolbox developed at University of California, Davis. The RGB image is converted into Hue, Saturation, and Value (HSV) by a Matlab subroutine. It is then possible to sample a profile from the hue image and obtain numerical values of hue along that profile.

For h contour plots, an image is converted to hue using Paint Shop Pro and other image editing software. Within the same software, the image is resized (maintaining the original height to width ratio) and a coordinate system drawn on the figure itself. Using a drawing tool, the yellow line, indicating the activation temperature, was traced onto the image. The image was then removed, and another image loaded for another heat transfer contour line.

3. Application to a protruding cylinder in cross-flow

A cylinder in cross-flow is a very common aerodynamic application and is therefore a well studied flow. For a cylinder in cross-flow, the vortex shedding frequency has been determined as a function of Reynolds number in terms of the Strouhal number ($St = fd/V$). For the cylinder in cross-flow, the Karman vortex street sheds with a nearly constant Strouhal number of 0.21 for Reynolds numbers between 4000 and 10,000.

3.1. Protruding cylinder in cross-flow images and results

Fig. 10 shows the hue of three sequential images on a surface downstream of a protruding 5 cm cylinder in cross-flow. The Strouhal number for these test conditions, suggests a shedding frequency of approximately 40 Hz, a value too high to capture with the current frame rate. The images do however, show distinct fluctuations from frame to frame and provide a demonstration of the ability to view the presence of dynamic behavior.

In Fig. 10 the entire surface is incident with a uniform heat flux and flow goes from left to right. The protruding cylinder acts as a bluff body to the flow and cooling is reduced in the wake of the cylinder. The blue color behind the cylinder indicates higher temperature as a result of lower heat transfer coefficients.

4. Application to flow downstream of a shallow surface cavity

Surface cavities, or dimples, have been recognized as a means of providing both passive flow control and heat transfer enhancements. Bearman and Harvey (1976) describe one of the most famous examples of spherical

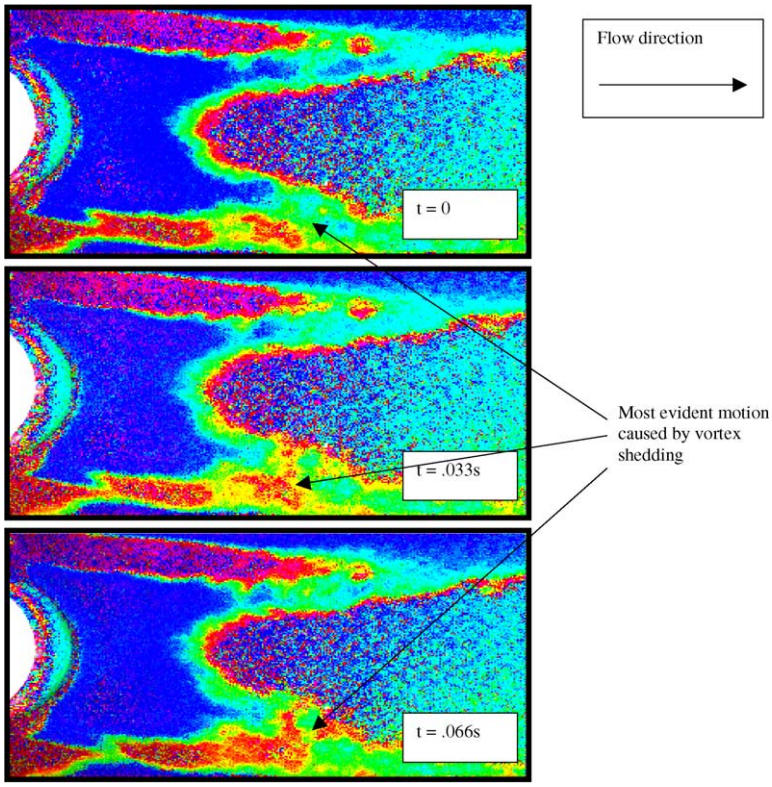

Fig. 10. Hue images from successive frames of a 5 cm protruding cylinder in cross-flow $Re_D = 38{,}330$ (flow left to right).

dimple applications which is a drag coefficient reduction on a dimpled golf ball compared to a smooth one. Improved aerodynamics is the result of energizing the boundary layer which delays flow separation. More recently, dimples are being considered for applications to low pressure turbine blades that suffer from reduced engine efficiency due to separation at low Reynolds conditions. Different dimple shapes, including an asymmetric dimple have been studied. Rouser (2002) has investigated local and average pressure drops for both a spherical and asymmetric dimple (a semi-circular spherical indention with a stream wise straight edge) on a modified Pak-B blade in a linear cascade wind tunnel for $Re_D = 25\,\text{K}$, 45 K and 100 K. He found both types of shallow cavities to transitioning a laminar boundary layer and thereby preserving an attached flow condition to the turbine blade. Ligrani et al. (2001) measured instantaneous, dynamic and time averaged characteristics of shed vortices due to dimples in a channel. Using smoke visualization, his team viewed vortices shed periodically from the center of the dimple for varying Reynolds numbers between 6000 and 11,000 (based on channel height). It was shown that the shedding frequency increased with higher channel heights giving dimple diameter-based Strouhal numbers between 0.1 and 0.16 (where a factor of 2 is removed for consistency in units here). Frequencies were less than 10 Hz for the maximum velocities in this investigation.

4.1. Cylindrical dimple images and results

For the present application a shallow cylindrical cavity with a depth to diameter ratio of 0.1 was placed upstream of the tissue surface. For all dimple images, flow is from left to right unless otherwise noted. Fig. 11a shows the liquid crystal image for $Re_D = 16{,}683$ at one heat flux. Fig. 11b shows the corresponding heat transfer coefficients calculated for this Reynolds number using Eq. (4). The uncertainty in the heat transfer coefficients is estimated to be 12–15%. There were no observable fluctuations in the heat transfer coefficients using this method. Hue analysis over a series of frames also showed no evidence of vortex shedding. This is not surprising since the Strouhal number of 1–2 reported by Khalatov et al. (2004) would suggest frequencies much higher than the frequency response of 100 Hz. It was interesting however that a slight asymmetry was apparent at low velocities ($Re_D = 5186 - 8294$), and continued to develop to a maximum asymmetry at $Re_D = 16{,}683$. When the Reynolds number was increased to 18,034, these asymmetries diminished as shown in Fig. 12a and b. Similar asymmetries were also observed by Khalatov et al. (2004) in a water tunnel visualization of spherical and cylindrical dimples. They also noticed that this occurred over a limited similar Reynolds number range. Note that in Figs. 11b and 12b, the range of heat transfer coefficients is obtained

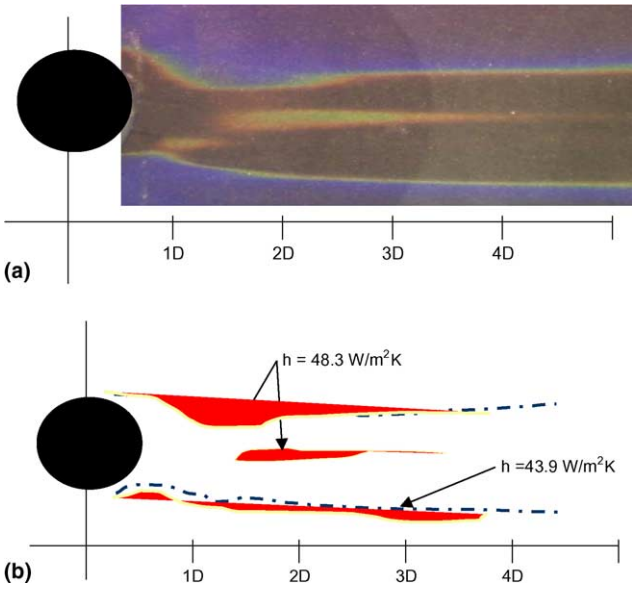

Fig. 11. (a) Asymmetric flow patterns downstream of a cylindrical dimple in RGB for $Re_D = 16{,}683$. (b) Asymmetric heat transfer coefficient distribution downstream of a cylindrical dimple from Fig. 11a.

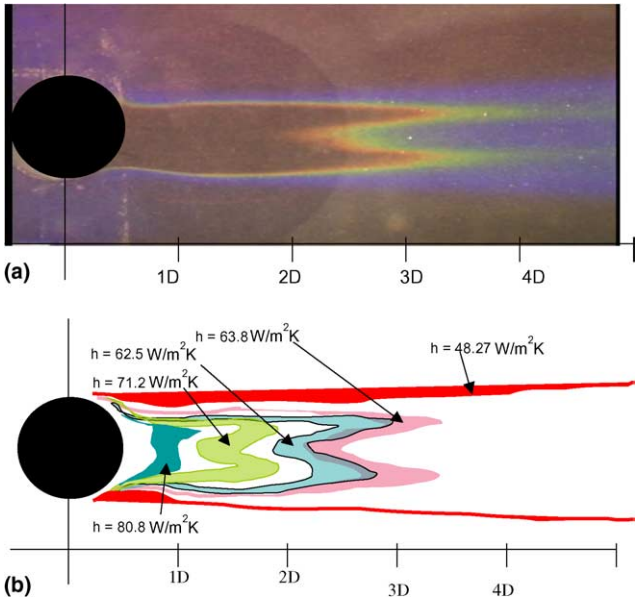

Fig. 12. (a) Symmetric flow patterns of a cylindrical dimple in RGB for $Re_D = 18{,}034$. (b) Symmetrical heat transfer coefficient distribution downstream of a cylindrical dimple from Fig. 12a.

by varying the radiant heat flux. An example of the change in the liquid crystal images when this is done is shown in Fig. 13.

5. Conclusions and summary

- A new method of surface flow visualization and transient heat transfer measurement technique has been demonstrated for oscillating flow conditions. The means of visualization is provided by liquid crystal thermography. Temperature changes are the result of fluctuating heat transfer coefficients due to vortex shedding, pulsating or unsteady flows.
- The response of the technique is dependent on the mass of the substrate, the color play temperatures of the liquid crystals, and the percent change in h. Given the mass of our tissue surface, the maximum detectable frequency by this method is 100 Hz, where image processing is required to determine changes in hue not detectable by the eye, but well within the ability of the liquid crystals to capture if the video frame rate is high enough.
- This method was demonstrated for two applications, a protruding cylinder in cross-flow and a surface with a cylindrical surface cavity.
  - The cylinder shedding frequency is a well studied phenomenon, For our test conditions; a frequency of greater than 20 Hz would be expected. This is too high a frequency to capture with our sampling rate of 30 Hz. What was captured however was distinct and observable dynamic behavior from frame to frame.
  - The cylindrical dimple in cross-flow showed no visible signs of shedding. Asymmetric behavior was observed for low Re, and disappeared at higher velocities as observed by Khalatov et al. (2004).

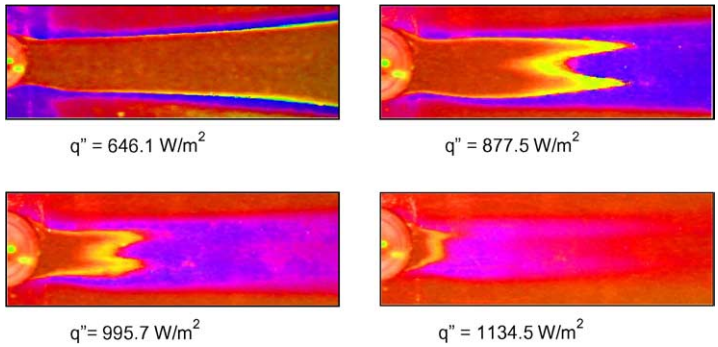

Fig. 13. The effect of heat flux setting on the hue images downstream of a cylindrical dimple $Re_D = 16{,}683$.

References

Baughn, J.W., 1995a. Liquid crystal methods for studying turbulent heat transfer. Int. J. Heat Fluid Flow 16, 365–375.

Baughn, J.W., Butler, R.J., Byerley, A.R., River, R.B., 1995b. An Experimental investigation of Heat Transfer, Transition and Separation on Turbine Blades at Low Reynolds Number and High Turbulence Intensity. ASME Paper 95-WA/HT-25, Proceedings Mechanical Engineering Congress and Expositions, San Francisco, CA, USA.

Bearman, P.W., Harvey, J.K., 1976. Golf ball aerodynamics. Aeronaut. Quart. 27, 112–122.

Byerley, A.R., Stormer, O., Baughn, J.W., Simon, T.W., Van Treuren, K., 2002. A "Cool" thermal tuft for detecting surface flow direction. ASME J. Heat Transfer 124, 194.

Critoph, R.E., Holland, M.K., Fisher, M., 1999. Comparison of steady state and transient methods for measurement of local heat transfer in plate fin-tube heat exchangers using liquid crystal thermography with radiant heating. Int. J. Heat Mass Transfer 42, 1–12.

Incropera, F.P., DeWitt, D.P., 2002. Fundamentals of Heat and Mass Transfer, 5th ed. John Wiley & Sons, New York, p. 398.

Ireland, P.T., Jones, T.V., 1986. Detailed measurements of local heat transfer on and around a pedestal in a fully developed passage flow. In: 8th International Heat Transfer Conference, 4, 975–980.

Jones, T.V., 1977. Heat transfer, skin friction, total temperature and concentration measurements. In: Richards, B.E. (Ed.), Measurements of Unsteady Fluid Dynamic Phenomena. McGraw Hill, Berlin, pp. 63–102.

Khalatov, A., Byerley, A., Ochoa, D., Min, S.K., 2004. Flow characteristics within and downstream of spherical and cylindrical dimple on a flat plate at low Reynolds numbers, ASME Turbo Expo 2004, Paper GT2004-53656.

Ligrani, P.M., Mahmood, G.I., Harrison, J.L., Clayton, C.m., Nelson, D.L., 2001. Flow structure and local Nusselt number variations in a channel with dimples and protrusions on opposite walls. Int. J. Heat Mass Transfer 44, 4413–4425.

Mayhew, J.E., Baughn, J.W., Byerley, A.R., 2003. The effect of freestream turbulence on film cooling adiabatic effectiveness. Int J. Heat Fluid Flow 24, 669–679.

Rivir, R.B., Baughn, J.W., Townsend, J.L., Butler, R.J., Byerley, A.R., 1999. Thermal Tuft Fluid Flow Investigation Apparatus with a Color Alterable Thermally Responsive Liquid Crystal Layer, United States Patent 5,963,292.

Rouser, K, 2002. Use of Dimples to Suppress Boundary Layer Separation on a low pressure Turbine Blade, M.S. Thesis, Air Force Institute of Technology.

Van Dyke, M., 1982. An Album of Fluid Motion. Parabolic Press, Stanford, CA.